Journal of Materials Chemistry A

Accepted Manuscript

ROYAL SOCIETY OF CHEMISTRY

www.rsc.org/materialsA

Journal Name Journal of Materials Chemistry A Dynamic Article Links ►

Cite this: DOI: 10.1039/c0xx00000x

www.rsc.org/xxxxxx

ARTICLE TYPE

Highly Stable Anion Exchange Membranes Based on Quaternized Polypropylene

Min Zhang[a], Jinling Liu[a], Yiguang Wang,*[a] Linan An[c] Michael D. Guiver,[d,e] and Nanwen Li*[b]

Received (in XXX, XXX) Xth XXXXXXXXX 2015, Accepted Xth XXXXXXXXX 20XX

DOI: 10.1039/b000000x

A series of novel quaternized polypropylene (PP) with 'side-chain-type' architecture was prepared by heterogeneous Ziegler-Natta catalyst mediated polymerization and subsequently quaternization. Tough and flexible anion exchange membranes were prepared by melt-pressing of bromoalkyl-functionalized PP (PP-CH_2Br) at 160 °C, followed by post-functionalization with trimethylamine (TMA) or N,N-dimethyl-1-hexadecylamine (DMHDA) and ion exchange. By the simple incorporation of a thermally-crosslinkable styrenic diene monomer during polymerization, crosslinkable PP-AEMs were also prepared at 220 °C. PP-AEM properties such as ion exchange capacity, thermal stability, water and methanol uptake, methanol permeability, hydroxide conductivity and alkaline stability of uncrosslinked and crosslinked membranes were investigated. Hydroxide conductivities of above 14 mS cm^{-1} were achieved at room temperature. The crosslinked membranes maintained their high hydroxide conductivities in spite of their extremely low water uptake (up to 56.5 mS cm^{-1} at 80 °C, water uptake = 21.1 wt %). The unusually low water uptake and good hydroxide conductivity may be attributed to the "side-chain-type" structures of pendent cation groups, which probably facilitate ion transport. The membranes retained more than 85 % of their high hydroxide conductivity in 5 M or 10 M of NaOH aqueous solution at 80 °C for 700 h, suggesting their excellent alkaline stability. It is assumed that the long alkyl spacer in 'side-chain-type' of 9 carbon atoms between polymer backbone and cation groups reduce the nucleophilic attack of water or hydroxide at the cationic centre. Thus, the PP-based AEMs with long "side-chain-type" cations appear to be very promising candidates with good stability for use in anion exchange membrane fuel cells (AEMFC)s.

Introduction

Anion exchange membrane fuel cells (AEMFCs) have been gaining significant interest over the past several years owing to their significant advantages of improved oxygen reduction and fuel oxidation kinetics, which can lead to higher efficiencies, while the alkaline environment allows utilization of non-precious metal catalysts, greatly reducing the device cost.[1–5] Although AEM technology has improved immensely in the past decade, AEM fuel cells continue to perform unfavorably compared to their PEM counterparts because of a significant performance gap of lower ionic conductivities and ineffective alkaline stability.

Given the high performance of PEM, it is evident that their structure and chemistry have significantly influenced AEM design. In the pursuit of hydrocarbon-based AEMs with improved properties, we and others have shown several promising approaches to enhance quaternary ammonium (QA)-based AEM properties and performance, which are (1) to position the QA group on side chains grafted onto the polymer main chain (side-chain-type), (2) to form comb-shaped quaternized PPO AEMs using a long alkyl chain of 6–16 carbon atoms pendant to the QA groups[6–10] and (3) to crosslink the AEM matrix by catalyzed or thermal crosslinking.[6,11,12] For example, AEMs with long alkyl chains of 6–16 carbon atoms grafted onto QA groups had improved alkaline stability. The steric hindrance effect of long alkyl chains was believed to effectively reduce nucleophilic attack of water or hydroxide at the QA centres, thereby improving alkaline stability. Recently, Hibbs and co-workers[13] reported similarly enhanced alkali stability for a poly(phenylene) with a 'side-chain-type' QA group attachment by hexamethylene spacers. Furthermore, polymer structures containing flexible pendent side chains linking the hydrophobic polymer with hydrophilic QA groups typically exhibit nanophase separation between hydrophilic and hydrophobic domains, enhancing hydroxide conductivity.

Additionally, the structure of the polymer backbone was observed to have a significant influence on the AEM properties and performance. For example, Ramani and coworkers[14] demonstrated the degradation of aromatic polysulfone backbone which arose from both the quaternary carbon and ether hydrolysis, using 2D NMR spectroscopy (correlation spectroscopy (COSY) and heteronuclear multiple quantum correlation spectroscopy (HMQC)). Subsequently, Hickner[15] et al. reported that quaternary ammonium groups displayed different

alkaline stabilities when attached to different polymer backbones, by comparison of the alkaline stabilities of quaternized poly(arylene ether sulfone) (PAES), poly(phenylene oxide) (PPO) and polystyrene (PS) using the quantitative ^{1}H NMR spectroscopy. It was observed that quaternized PS offered a significant increase in stability over quaternized PAES. Therefore, to render the cations and backbone less susceptible to degradation in alkaline environment, the design of both the cation and the selection of polymer backbones are crucially important.

Polyolefins, such as high density polyethylene (HDPE) or isotactic polypropylene (*i*PP), are known to be highly stable in alkaline[38] and in electrochemical environments, such as rechargeable lithium ion batteries.[16–18] Several polyolefin-based ion exchange membranes have been reported.[19–21] However, because of synthetic difficulties – catalyst poisoning[22,23] by functional groups in the direct Ziegler-Natta mediated α-olefin polymerization process, most functionalized polyolefins have been prepared by post-functionalization, such as irradiation-mediated free radical graft polymerization with functionalized monomer. Unfortunately, post-functionalization of free radical graft polymers usually results in very complicated molecular structures which have rarely been characterized.[24] Recently, Chung and co-workers[25,26] reported the preparation of amino-functionalized polyolefins from silane-protected α,ω-aminoolefin via metallocene catalyst mediated copolymerization. The quaternized polyethylene-based AEM having 'side-chain-type' quaternary ammonium groups was obtained by interconverting the silane-protected amino groups. High ionic conductivities of 119.6 mS/cm in 2 M HCl were observed. In addition, Coats et al.[27] used ring-open metathesis polymerization (ROMP) with functionalized monomer and subsequent hydrogenation reaction to prepare solution-processable uncrosslinked PE-based AEMs, which exhibited a high hydroxide conductivity of 65 mS·cm^{-1} at 50 °C. They further[28] developed this synthetic approach to prepare cross-linked AEMs via ring-opening metathesis copolymerization of cyclo-olefins and their quaternary-ammonium derivatives. However, the crosslinked unsaturated ROMP polymer, in which the unsaturated double bonds might not be alkaline stable, was not susceptible to hydrogenation. Isotactic polypropylene (PP) structures usually possess higher mechanical properties, higher melting temperatures and better film-forming capabilities than those of PE, which makes PP a viable candidate for AEMs application. To the best of our knowledge, there are few reports related to PP based AEMs, which is probably because a smaller selection of comonomers that can be incorporated into the PP backbone in high molar ratio in comparison with relatively less reactive ethylene monomer.[22,23]

The objective of the present research is the preparation and systematic property evaluation of AEMs based on the highly stable polypropylene backbone containing "side-chain-type" QA groups. PP copolymer with a bromoalkyl side chain was first synthesized via Ziegler-Natta catalyzed copolymerization of propylene and 11-bromo-1-undecene. Subsequent conversion of the bromoalkyl to quaternary ammonium by treatment with trimethylamine (TMA) or N,N-dimethyl-1-hexadecylamine (DMHDA) and ion exchange reaction provided a PP-AEM with hydroxide-conductive properties. Crosslinked AEM was also prepared by introduction of crosslinkable diene monomer and subsequent thermal crosslinking. The properties of the resulting membranes, such as the alkaline stability, mechanical strength, water uptake behaviour, methanol permeability, and hydroxide conductivity were investigated in detail.

Experimental Section

Materials

All O_2 and moisture sensitive manipulations were carried out inside an argon filled Vacuum Atmospheres dry-box. Polymerization-grade propylene was used as received. $TiCl_3$·AA, $AlEt_2Cl$ (10 wt% in toluene), trimethylamine (TMA) solution (~45 wt% in H_2O), N, N-dimethyl-1-hexadecyamine (DMHDA), 11-bromo-1-undecene, calcium hydride and heptanes were purchased from Sigma-Aldrich. Other chemicals, including methanol, sodium hydroxide, allylmagnesium bromide (1.0 M solution in diethyl ether), diethyl ether (anhydrous), 4-vinylbenzyl chloride and hydrochloric acid were analytical grade and were also from Sigma-Aldrich and used as received. Heptane was distilled over sodium/potassium alloy with benzophenone as indicator under argon gas protection. 11-Bromo-1-undecene was distilled over CaH_2 under reduced pressure before use.

Synthesis of crosslinker *p*-(3-butenyl)styrene (BSt)

To a dry 500 mL three-necked round-bottom flask equipped with addition funnel, condenser, and magnetic stir bar was transferred 200 mL (0.2 mol) of allylmagnesium bromide solution. A 20 mL (0.14 mol) aliquot of 4-vinylbenzyl chloride diluted with 50 mL of diethyl ether was added dropwise to allylmagnesium bromide at ice bath temperature. After complete addition of 4-vinylbenzyl chloride, the mixture was warmed to room temperature and refluxed for 12 h. Then, 200 mL of distilled water was slowly added to the mixture. The aqueous layer was separated and washed three times with diethyl ether. The organic phases were combined and dried with anhydrous sodium sulfate. After evaporation of the solvent the residue was further dried with calcium hydride and distilled under vacuum before use. Yield: 20.1 g, 94%. ^{1}H NMR spectrum: δ 7.1–7.5 (m, 4 H, phenyl−H), 6.7 (m, 1 H, phenyl−C*H*=CH$_2$), 5.9 (m, 1 H, −C*H*=CH$_2$), 5.7 (d, 1 H, phenyl−CH=C*H*$_2$), 5.3 (d, 1 H, phenyl −CH=C*H*$_2$), 5.1 (m, 2 H, −CH=C*H*$_2$), 2.7 (t, 2 H, phenyl−C*H*$_2$), 2.4 (m, 2 H, −C*H*$_2$−CH=CH$_2$).

Synthesis of functionalized polypropylene without crosslinkable groups

In a typical copolymerization reaction, 100 mL of heptanes was charged into a Parr 450 mL stainless autoclave equipped with a mechanical stirrer in a dry-box. After removal from the box, the reactor was injected with a certain amount of 11-bromo-1-undecene as comonomer and then charged with 20 psi (~1.4 atm) of propylene to saturate the heptane solution at 70 °C. About 0.4 g of $TiCl_3$·AA and 5.0 mL of $AlEt_2Cl$ (10 wt% in toluene) was mixed together and stirred for 30 minutes in the dry-box at room temperature to activate the catalyst and then injected into the reactor under rapid stirring to initiate the copolymerization. Additional propylene was fed continuously into the reactor to maintain a constant pressure (20 psi) during the entire course of the polymerization. After a certain reaction time elapsed at 70 °C, the reaction solution was quenched by methanol, followed by pouring the polymer solution into acidic methanol solution. The polymer, denoted as PP-Br, was filtered and washed with THF

and methanol thoroughly and dried under vacuum at 60 °C for 12 h.

Synthesis of functionalized polypropylene with crosslinkable groups

Terpolymerization of propylene with 11-bromo-1-undecene and *p*-(3-butenyl)styrene was carried out under similar procedures. 100 mL of heptanes was charged into a Parr 450 mL stainless autoclave equipped with a mechanical stirrer in a dry-box. After removal from the box, a certain amount of 11-bromo-1-undecene and *p*-(3-butenyl)styrene were sequentially introduced into the autoclave under propylene atmosphere (20 psi). About 0.4 g of $TiCl_3$·AA and 5.0 mL of $AlEt_2Cl$ (10 wt% in toluene) was mixed together and stirred for 30 minutes in the dry-box and then injected into the flask under rapid stirring to initiate the polymerization at 70 °C. After 60 minutes at 70 °C, the reaction solution was quenched by methanol, followed by pouring the polymer solution into acidic methanol solution. The polymer, denoted as nx-PP-Br, was filtered and washed with THF and methanol thoroughly and dried under vacuum at room temperature for 12 h.

Evaluation of crosslinking efficiency

The resulting crosslinkable terpolymer nx-PP-Br was dissolved in xylene at 130 °C, and the heated polymer solution was directly cast into films (thickness 10–20 μm) at 125 °C. The resulting films were then heated in a vacuum oven at 220 °C for 15 minutes. The resulting cross-linked films were subjected to vigorous Soxhlet extraction with refluxing xylene for 24 h under argon to ensure removal of the soluble polymer fraction before drying the films and determining the gel content. The gel fraction of the crosslinked membranes was calculated by measuring the residual mass of the sample and then computed by the equation: gel fraction = $(W_d / W_i) \times 100\%$, where W_i is the initial weight of dried membranes and W_d is the weight of the dried insoluble fraction of membranes after extraction.

Membrane Preparation

Membranes were prepared by hot-press processing at 160 °C under a pressure of 24000 psi to remove defects, providing an average thickness in the range of 40–60 μm. In the nx-PP-Br terpolymer case, the membranes were further treated at 220 °C for 15 minutes under vacuum to complete the crosslinking reaction.

Quaternization and Ion Exchange

PP-Br membranes in vials were stirred in about 30 mL of 45% aqueous solution of TMA or DMHDA at about 35–40 °C for 36 h. After completion of the reactions, the membranes were washed with deionized water to remove excess TMA or DMHDA and then dried at 60 °C overnight, followed by vacuum at 70 °C for 8 h. The obtained membranes were treated with 1 M NaOH solution at room temperature for 48 h to obtain PP-R-y (R = TMA or DMHDA, y = Br content incorporated). The membranes were washed thoroughly to remove residual NaOH and stored in DI water prior to analysis. The nx-PP-Br terpolymer film samples after thermal crosslinking at 220 °C were quaternized and ion exchanged using similar procedure; the samples were denoted as x-PP-R-y (R = TMA or DMHDA, y = Br content incorporated).

Membrane characterization

All high-temperature ^{1}H NMR spectra were recorded on a Bruker AM-300 instrument in 1,1,2,2-tetrachloroethane-d_2 at 110 °C. The polymer molecular weights were also analyzed on a PL-220 series high temperature gel permeation chromatography (GPC) unit equipped with four PLgel Mixed-A (20μm) columns (Polymer Laboratory Inc.). The oven temperature was at 150 °C and the temperatures of the autosampler's hot and the warm zones were at 135 °C and 130 °C respectively. The solvent 1,2,4-trichlorobenzene (TCB) containing ~200 ppm tris(2,4-di-tert-butylphenyl) phosphite (Irgafos 168) was nitrogen purged. The flow rate was 1.0 mL/min and the injection volume was 200 μL. A 2 mg/mL sample concentration was prepared by dissolving the sample in N_2 purged and preheated TCB (containing 200 ppm Irgafos 168) for 2.5 h at 160 °C with gentle agitation. The melting temperatures of the polymers were measured by differential scanning calorimetry (DSC) using a Perkin-Elmer DSC-7 instrument controller with a heating rate of 20 ^{o}C/min. Thermal stability of the samples were investigated by using a TA instrument thermogravimetric analyzer (TGA) instrument model TA SDT Q600. Preheating of the polymer samples was performed at 100 °C for 40 min under argon atmosphere to remove moisture. Small amounts of polymer were placed in ceramic cells and the temperature was increased from 30 to 700 °C under nitrogen atmosphere with a heating rate of 20 °C/min. Fourier transform infrared spectroscopy (FTIR) was recorded on a PE-1710 spectrometer from 4000 to 400 cm^{-1} with a 4 cm^{-1} resolution in 64 scans using polymer thin films. All mechanical properties (tensile strength, tensile modulus, elongation at break, etc.) were measured according to the ASTM D-1708 method. The dog-bone specimens (38 mm × 15 mm overall size and 5 mm × 22 mm in the gauge area) were die cut and performed using an Instron 5866 universal tester, with a load cell of 100 N and a constant cross head speed of 1 mm/min. At least 6 samples were tested in order to minimize possible errors. To assess the chemical stability, anion exchange membrane samples of 5 cm diameter were immersed in 5 M and 10 M NaOH solution at 80 °C for time period ranging 0~700 h. After contact, the membranes samples were separated, and washed with DI water until the absence of the alkalinity in the effluent, followed by IEC determination and conductivity measurement.

Small-angle X-ray scattering curves of unstained dry membranes were obtained using a Rigaku (formerly Molecular Metrology) instrument equipped with a pinhole camera with an Osmic microfocus Cu Ka source and a parallel beam optic. Typical counting times for integration over a multiwire area detector were 1 h with typical membrane thicknesses on the order of 100 m. Measurements were taken under vacuum at ambient temperature on dry samples. Scattering intensities were normalized for background scattering and beam transmission.

Ion-Exchange Capacity (IEC)

The ion-exchange capacities (IECs) of the membranes were measured in triplicate using a typical titration method. Accurately weighed samples in OH^- form were immersed into 25 mL of 0.05 M HCl solution and equilibrated for 48 h under argon atmosphere, after which the HCl solution was back titrated by 0.05 M NaOH

solution using phenolphthalein as indicator. IEC values of the samples were calculated using the following equation:

$$\mathrm{IEC} = \frac{n_1 \cdot \mathrm{HCl} - n_2 \cdot \mathrm{HCl}}{M_{\mathrm{dry}}} (\mathrm{meq} \cdot \mathrm{g}^{-1})$$

Where n_1·HCl and n_2·HCl are the amounts (mmol) of hydrochloric acid required before and after equilibrium respectively, and M_{dry} is the mass (g) of the dried sample. The average value of the three samples calculated from the above equation is the IEC value of the measured membrane.

Water and Methanol Uptake

The water and methanol uptake of the previously vacuum dried membranes were measured for 24 h in DI water and methanol, respectively. The reported measurements are based on the average of two readings of each sample of dimension about 30 mm × 30 mm. Water uptake was measured at 20, 30, 40, 50, 60, 70 and 80 °C while methanol uptake was measured at 20 °C. The temperature was controlled by means of a thermostatic water bath. The weight percentage uptake W(%) was determined by the following equation:

$$W(\%) = \frac{(W_{\mathrm{w}} - W_{\mathrm{d}})}{W_{\mathrm{d}}} \times 100\%$$

where W_{d} and W_{w} are the weight of the dry and fully hydrated membrane, respectively.

The swelling ratio was characterized by the linear expansion ratio, which was determined by the difference between the wet and dry dimensions of membrane samples after immersion in water at 20, 30, 40, 50, 60, 70 and 80 °C for 24 h (4 cm in length and 1 cm in width). The calculation was based on the following equation:

$$\mathrm{Swelling}(\%) = \frac{X_{\mathrm{wet}} - X_{\mathrm{dry}}}{X_{\mathrm{wet}}} \times 100\%$$

With the obtained weight percentage uptake W(%) and IEC value, the hydration number (λ) was calculated by following equation:

$$\lambda = \frac{W(\%) \times 10}{\mathrm{IEC} \times 18}$$

Methanol Permeability

Methanol permeability (P, $\mathrm{cm}^2 \cdot \mathrm{s}^{-1}$) was measured at 30 °C using a two-chamber diffusion cell method. Prior to the measurement, each membrane coupon (diameter = 2.5 cm) was soaked in water to the fully hydrated state for at least 1 day. One chamber (80 mL) contained 10 M (34 wt %) methanol solution and the other chamber (80 mL) was filled with DI water. The diffused methanol was periodically measured using a Shimadzu GC-1020A series gas chromatography machine. Peak areas were converted into methanol concentration with a calibration curve. The methanol concentration in the receiving compartment as a function of time is given by the following equation:

$$C_B(\mathrm{t}) = \frac{A}{V_B} \times \frac{DK}{L} \times C_A \times (\mathrm{t} - \mathrm{t}_0)$$

where C_{A} and C_{B} are methanol concentrations of the membrane feed side and permeate side, respectively. A, L and V_{B} are the effective membrane area, thickness and the liquid volume of permeate compartment, respectively. DK is defined as the methanol permeability and t_0 is the time lag.

Hydroxide Conductivity

AC impedance spectroscopy was used to measure the membrane conductivity on a Solartron SI 1260A Impedance/Gain-Phase Analyzer and an electrochemical interface (Solartron 1287, Farnborough, Hampshire, UK). The electrode system was installed in an electrically shielded thermo- and hygro-controlled chamber. The impedance measurement was carried out at a given temperature and relative humidity (RH). The OH^- conductivity (σ) was obtained from the following equation:

$$\sigma_{OH^-}(\mathrm{S} \cdot \mathrm{cm}^{-1}) = \frac{L}{RA}$$

where σ is the hydroxide conductivity ($\mathrm{S} \cdot \mathrm{cm}^{-1}$, R is the ohmic resistance of the membrane sample (Ω). L is the distance between the electrodes to measure the voltage drop (cm), and A is the cross-sectional area of the membrane samples (cm^2). In order to avoid the effect of carbonation, the membranes were converted to OH^- form and washed just before the conductivity measurement. Moreover, the tests were also conducted in water which minimizes the exposure to air. The impedance of each sample was measured repeatedly to ensure reproducibility for the measured data.

Fuel Cell Performance Evaluation

A well-dispersed catalyst ink was prepared by mixing 46.4 wt% Pt/C catalysts (TKK, Japan) with de-ionized water, 1-propanol and AS-4 (Tokuyama Corporation, Japan) ionomer solution (5 wt% in 1-propanol) using magnetic stirring and ultrasonication. To obtain a catalyst-coated substrate (CCS) for the electrodes, the as-prepared ink was coated onto the surface of SGL 25BC carbon paper (SGL group, Germany) using an air spray gun (Iwata, Japan). The Pt loading and ionomer content in the catalyst layer were ~0.60 $\mathrm{mg/cm}^2$ and ~20 wt.%, respectively. Anode CCS, PP-TMA-20 membrane (Tokuyama Corporation, Japan) and cathode CCS were assembled together in a cell fixture to form a membrane/electrode assembly (MEA). The electrode size was 2.25 cm × 2.25 cm (~5 cm^2). Fuel cell testing was conducted with a commercial fuel cell (Teledyne, USA) testing system at 50 °C and 100 RH %. Fully humidified hydrogen was supplied to the anode at 500 SCCM as indicated in the data, while fully humidified oxygen was supplied to the cathode at 500 SCCM. After full activation of the MEA for 1 h, the fuel cell polarization curve was measured under galvanostatic mode, i.e. holding the fuel cell at serial constant currents (for example, 50, 100 and 250 $\mathrm{mA/cm}^2$, etc.) for 3 min. The cell voltage as a function of current density was recorded using fuel cell testing software.

Results and Discussion

Synthesis and Characterization of Bromoalkyl-Functionalized Polypropylene

Anion exchange membranes based on quaternized polypropylene derived from bromoalkyl functionalized polypropylene precursor (PP-Br) were synthesized using Ziegler-Natta catalyst mediated copolymerizations of propylene and 11-bromo-1-undecene, as shown in Scheme 1. While it is general known that polar monomers deactivate the Ziegler-Natta catalysts commonly used for the polymerization of olefinic hydrocarbons.[29] there are examples reported in the literature where compounds containing atoms with unshared electron pairs do not interfere with the polymerization. Bacskai and coworkers[30] reported that 8-bromo-1-octene could be incorporated into polypropylene using Ziegler catalyst catalyzed copolymerization, but only in around 7.0 mol % content. Herein, in comparison with 8-bromo-1-octene possessing 6 carbon atoms as spacer, 11-bromo-1-undecene with a longer spacer of 9 carbon atoms was selected because of its higher flexibility, which should allow it to be able to compete with less bulky and reactive propylene during copolymerization and therefore incorporate a higher molar ratio of bromoalkyl moieties. Table 1 summarizes the reaction conditions, polymer yield and properties. Although the catalyst activity systematically decreased with the increase of the feed content of 11-bromo-1-undecene, the PP-Br showed a favorably high molecular weight (M_w > 129 kg/mol) (Table 1 and Fig. S1) and typical PDI (5.7–7.0) resulting from commercially available Ziegler-Natta catalyst, namely $TiCl_3$·AA. Moreover, a higher concentration of bromoalkyl functionalized propylene in the PP-Br copolymer was also achieved (7.4–20.8 mol %). As shown in Fig. 1, the signal at 3.49 ppm could be attributed to the chemical shift of methylene next to bromine. Three major signals at 0.95, 1.35 and 1.65 ppm, correspond to methene, methylene and methyl groups respectively in the PP chain. The concentration of bromoalkyl in resulting copolymer PP-Br was calculated to be as high as 20.8 mol % according to the ^{1}H NMR results, when the monomer concentration was 1.2 M and reaction time increased to 60 min. By introduction of the crosslinkable monomer *p*-(3-butenyl)styrene (Bst) during the copolymerization, crosslinkable nx-PP-Br polymer with 20.1 mol % of bromoalkyl was also synthesized. As shown in Fig. 1b, there are several minor chemical shifts that are associated with the incorporated BSt comonomer units, including three distinct olefinic proton chemical shifts at 6.7, 5.7, and 5.2 ppm and two equal intensity aromatic proton signals at 7.1–7.2 and 7.3–7.4 ppm. With their relative chemical shift intensities, it is clear that most of the incorporated BSt units in the copolymer contain pendent styrene moieties. The integrated intensity ratio of the chemical shifts between 0.9 and 1.7 ppm and the chemical shifts between 7.1–7.4 ppm, and the number of protons that both chemical shifts represent, determines the concentration of BSt in the copolymers to be 0.7 mol %.

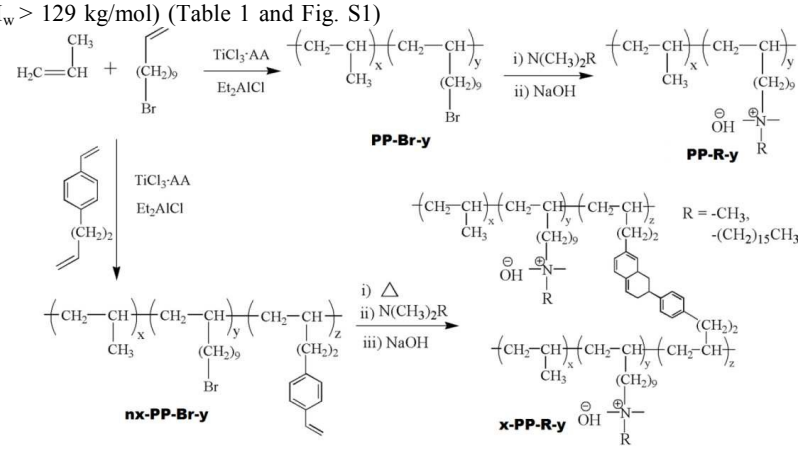

Scheme 1 The synthesis of PP-R-y and x-PP-R-y membranes (R = TMA or DMHDA; y = Br content incorporated; nx: non-crosslink; x: crosslink).

Table 1 Summary of Ziegler-Natta catalyst mediated copolymerization reaction between propylene, 11-bromo-1-undecene (M_1) and crosslinker *p*-(3-butenyl)styrene (M_2)

Samples [a]	Polymerization Conditions				Copolymerization results						
	Propylene (psi)	M_1 [b] (M)	M_2 [b] (M)	Time (min)	Yield (g)	$[M_1]$[c] (mol%)	$[M_2]$[c] (mol%)	M_w[d] (Kg/mol)	PDI[d]	T_m[e] (^{0}C)	ΔH[e] (J/g)
PP	20	0	0	30	10.5	0	0	590	5.7	162.9	78.9
PP-Br-7	20	0.2	0	30	6.4	7.4	0	386	6.1	150.4	53.8
PP-Br-20	20	1.2	0	60	2.6	20.8	0	148	6.6	115.3	31.6
nx-PP-Br-20	20	1.2	0.1	60	2.3	20.1	0.7	129	7.0	114.1	27.9

[a] General conditions: 0.4 g of $TiCl_3$•AA, 5 ml of Et_2AlCl, 100 ml of heptanes, reaction temperature: 70 ºC; [b] M_1: 11-bromo-undecene, M_2: *p*-(3-butenyl)styrene (BSt); [c] Comonomer content (mol%) in the *co*- and *ter*-polymers determined by ^{1}H NMR under 110 °C in 1,1,2,2-tetrachloroethane-d_2; [d] Weight-average molecular weights and polydispersity index were determined by GPC at 150 °C in 1,2,4-trichlorobenzene *vs* narrow polystyrene standards; [e] Melting temperature and heat of fusion determined by DSC.

Cite this: DOI: 10.1039/c0xx00000x

www.rsc.org/xxxxxx

ARTICLE TYPE

Membrane Preparation and Ion Exchange Capacity (IEC)

Although the molecular weights of PP-Br and nx-PP-Br were much lower than homopolymer PP (Table 1), tough and flexible membranes were obtained by melt hot-press processing at 160 °C under vacuum. Further thermal treatment of nx-PP-Br film at 220 °C under vacuum for 15 min led to crosslinked x-PP-Br membrane by cycloaddition between two pendant styrene units.[31] The crosslinking was further confirmed by the high gel-fraction (> 91.7 % under xylene extraction at 130 °C for 24 h). As shown in Fig. S5 and S6, the thermal regiospecific [2+4] cycloaddition reaction between two styrene units starts at a relatively low temperature (~80 °C) and achieves a high degree of crosslinking at 220 °C after about 20 min. Subsequently, the PP-Br and x-PP-Br membranes were quaternized with TMA or DMHDA aqueous solution by the Menshutkin reaction to get anion conductive membranes. The obtained membranes in the bromide salt form were then treated with 1 M aqueous NaOH at room temperature for 24 h to produce anion exchange membranes. There was no evidence of polymer chain degradation occurring under these conditions, as indicated by the mechanical properties of resulting polymer membranes. Fig. 2 shows the ^{1}H NMR spectrum of PP-DMHDA-7 in the hydroxide form. Comparison of PP-DMHDA-7 with its parent copolymer PP-Br-7 revealed that the signals assigned to the non-quaternized methylene groups at 3.49 ppm changed to much smaller in PP-DMHDA-7, while the polymer main-chain protons remained after the quaternized reaction. The new signals assigned to the methylene and methyl groups in quaternary ammonium appeared at 3.35 ppm in PP-DMHMA-7. However, the signal at 3.49 ppm did not disappear completely, which indicates the incomplete conversion of bromoalkyl to quaternary ammonium groups. Thus, the IEC values of PP-DMHDA-7 membranes were readily calculated to be 0.91 meq g^{-1} by comparing the integration ratios of the individual signals, which correlated well with the titrated value 0.87 meq g^{-1} (Table 3), but apparently lower than its theoretical value of 1.26 meq g^{-1}.

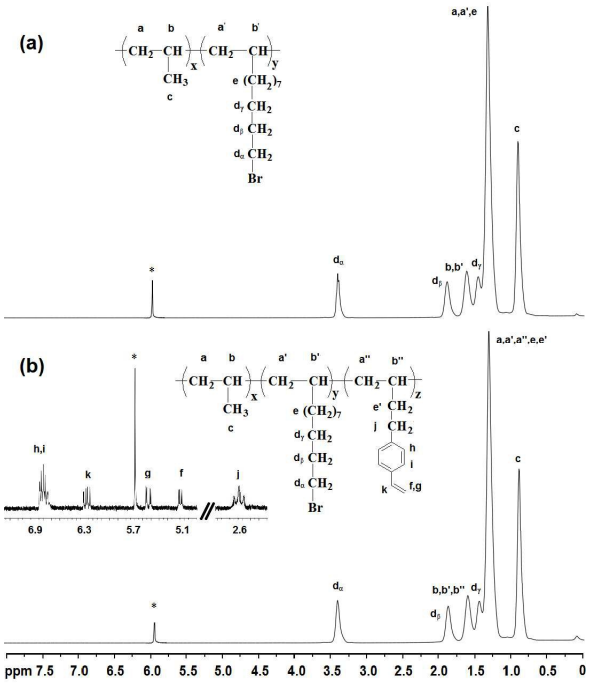

Fig. 1 ^{1}H NMR spectra of (a) PP-Br-20 and (b) nx-PP-Br-20 in 1,1,2,2-tetrachloroethane-d_2.

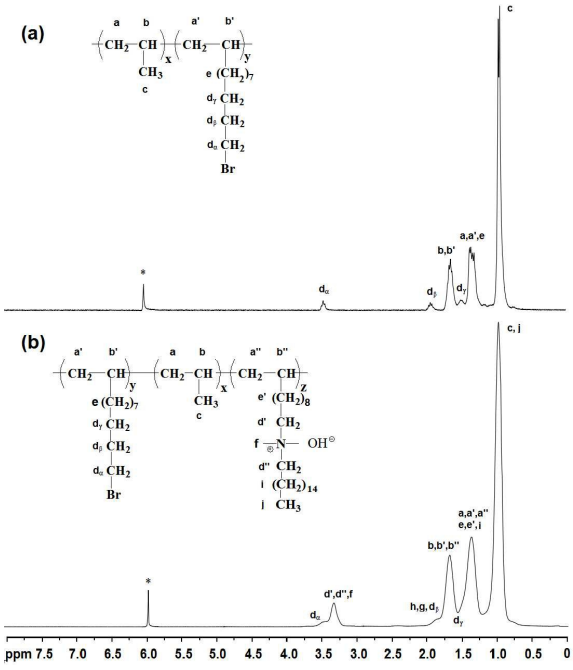

Fig. 2 ^{1}H NMR spectra of (a) PP-Br-7 and (b) PP-DMHDA-7 membrane in the hydroxide form in 1,1,2,2-tetrachloroethane-d_2.

The ^{1}H NMR spectra of PP-TMA-20 and PP-DMHDA-20 were not able to be obtained due to their poor solubility in organic solvent. However, the chemical structures of PP-AEMs were further analyzed by FT-IR spectra, as shown in Fig. 3 and Fig. S2. The absorption bands in the ranges of 2825–2870 cm^{-1} and 2870–2965 cm^{-1} are characteristic of symmetric and asymmetric stretching of aliphatic –CH_2 and –CH_3 groups, while C–H stretching and bending absorption bands for PP-based polymer appeared at 1472 cm^{-1} and 1463 cm^{-1}, respectively. The C–N stretching bands at 1100 cm^{-1} and 1126 cm^{-1} in x-PP-TMA-20 and x-PP-DMHDA-20 supported successful quaternization of the membrane. Furthermore, the broad absorption band in the range of 3400–3200 cm^{-1} in x-PP-DMHDA-20 and x-PP-TMA-20 membranes is attributed to O–H stretching in H_2O. These spectral features further supported that high concentration of –Br group was incorporated into the PP-based membrane and subsequently quaternized with TMA or DMHDA to form anion conductive membranes. The experimentally obtained IEC values of the membranes were titrated to be 1.48 and 1.42 meq. g^{-1} for PP-DMHDA-20 and x-PP-DMHDA-20 respectively, which was lower than the calculated values (1.66 and 1.65 meq. g^{-1}) from the copolymer composition and the degree of bromination further suggesting that incomplete quaternization of the bromoalkyl groups occurred. Moreover, the titrated IEC values of PP-TMA-20 and x-PP-TMA-20 membranes based on TMA (1.56 and 1.34 meq g^{-1} respectively) are also apparently lower than the theoretical values 2.56 and 2.33 meq g^{-1} (based on the degree of functionality assuming 100% amination efficiency, 100 % conversion to hydroxide form, and 100 % water removal when drying). The values determined by titration were between 58 % and 61 % of the calculated values, which could be attributed to incomplete conversion of bromoalkyl groups to quaternary ammonium groups. The similarly incomplete amination has been observed previously in chloromethylated poly(arylene ether sulfone).[32]

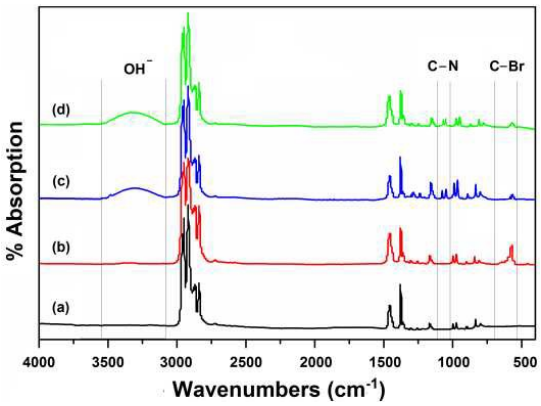

Fig. 3 FT-IR spectra of (a) PP, (b) nx-PP-Br-20, (c) x-PP-DMHDA-20 and (d) x-PP-TMA-20 membranes in the hydroxide form.

Thermal and Mechanical Properties

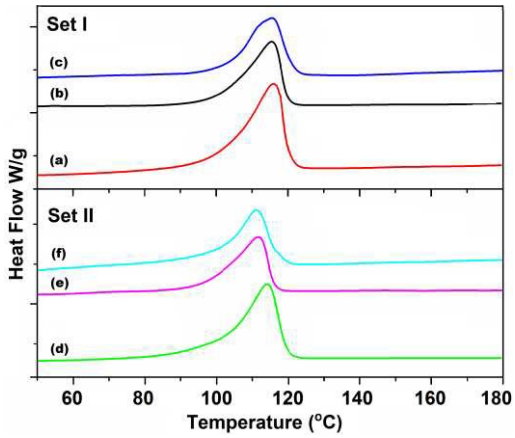

Fig. 4 DSC thermograms of set **I** (top): a) PP-Br-20 copolymer (T_m=115.3 °C, ΔH=31.6 J/g), b) PP-TMA-20 (T_m=115.1 °C, ΔH=27.1 J/g) and c) PP-DMHDA-20 membranes (T_m=115.0 °C, ΔH=25.4 J/g); set **II** (bottom): d) nx-PP-Br-20 (T_m=114.1 °C, ΔH=27.9 J/g), e) x-PP-TMA-20 (T_m=111.2 °C, ΔH=21.2 J/g) and f) x-PP-DMHDA-20 (T_m=111.5 °C, ΔH=20.3 J/g) membranes.

The DSC curves of PP-Br-20 copolymer and two corresponding membranes PP-TMA-20, PP-DMHDA-20 in the hydroxide form are shown in set **I** of Fig. 4 respectively ((a)–(c) from bottom to top). The endothermic peak at 115.3 °C represents the T_m of PP-Br-20 copolymer. Negligible decreases in T_m transition were observed after quaternization, indicating the original crystallites in the modified membranes remained intact, since T_m is a function of changes in the crystalline structure. Meanwhile, quaternization and subsequent ion exchange results in a dilution effect on the crystallinity of the copolymer, which leads to significant decreases in the areas (equal to ΔH values) under the curve. The DSC curves in set **II** ((d)–(f) from bottom to top) exhibit the nx-PP-Br-20, x-PP-TMA-20 and x-PP-DMHDA-20 after thermal cross-linking reaction, quaternization and ion exchange. As shown in Fig. 4 set **II**, the cross-linking slightly reduced T_m and crystallinity. For instance, the T_m of nx-PP-Br-20 was 114.1 °C, which was slightly higher than that of crosslinked x-PP-TMA-20 (T_m=111.2 °C) and x-PP-DMHDA-20 (T_m=111.5 °C). Significant decreases of ΔH values were also observed after cross-linking or quaternization, which could be contributed to both the cross-linking induced crystallinity reduction effect and dilution effect from quaternization.

The thermal stability of the membranes in their hydroxide form was evaluated by TGA under argon atmosphere. As shown in Fig. 5, there was no weight loss up to 165 °C, because all the samples were pre-heated at 120 °C for 12 h to remove absorbed water. As a control experiment, the thermal stability of PP and nx-PP-Br-20 was also compared by TGA. The PP and nx-PP-Br-20 showed excellent thermal stability. The main chain initial degradation temperature was up to 310 and 360 °C respectively. A two-step degradation profile was observed for quaternized PP copolymers in their hydroxide form (Fig. 5). The first weight loss occurred above 165 °C, which is associated with the degradation of the quaternary ammonium groups. This degradation temperature is higher than typically encountered quaternized aromatic polymers, such as quaternized PPO (~145 °C).[7] The high decomposition

temperature suggests that quaternary ammonium groups attached to pendent alkyl have better thermal stability. The main weight loss at around 310–450 °C is related to the degradation of the polymer chain. The decomposition temperature of the polymer backbone was similar with its parent polymer, suggesting that the decomposition of the quaternary ammonium groups did not trigger degradation of the polymer backbone, which has been observed in some aromatic AEMs.[33]

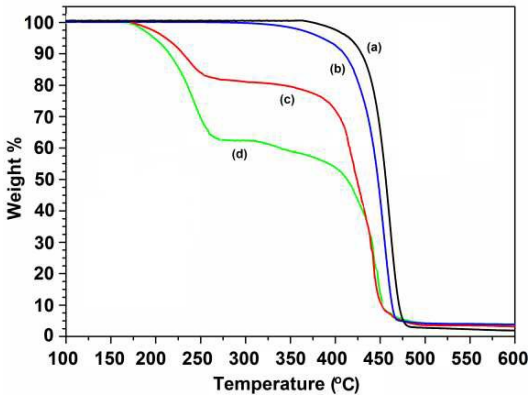

Fig. 5 TGA curves of (a) PP and (b) nx-PP-Br-20, (c) x-PP-TMA-20 and (d) x-PP-DMHDA-20 membranes in their hydroxide form.

The mechanical properties of the membranes are shown in Table 2. It is well known that PP film has good mechanical properties. Although the introduction of bromoalkyl during copolymerization decreased the molecular weight of PP to some extent (as discussed above, Table 1), the PP-Br-20 and nx-PP-Br-20 still had sufficiently high molecular weight and exhibited excellent mechanical properties. The membranes displayed values of tensile strength at maximum load of 16–21 MPa, Young's moduli of 0.58–0.78 GPa, and values of elongation at break of 310–350 %. These results indicate that PP-Br precursor membranes were tough and flexible for quaternization as AEMs. Furthermore, the slightly lower tensile strength, Young's modulus and elongation at break for quaternized PP AEMs was observed compared to their corresponding precursor polymers. Like previously reported ion-containing aromatic copolymers,[33] in which the ionic groups induced lower tensile strength and Young's modulus due to plasticization from absorbed water, the quaternization tended to decrease the mechanical properties, as shown in Table 2. However, the crosslinked quaternized x-PP-TMA-20 and x-PP-DMHDA-20 membranes had tensile strengths of ~ 62 MPa and Young's moduli of more than 1.5 GPa (Table 2). These values are much higher than that of precursor nx-PP-Br-20 or even PP due to the more compact chain architecture results from the crosslinking.[41] Similar behavior was also observed in crosslinked quaternized aromatic copolymers.[42,43]

Table 2 Summary of mechanical properties of the polymers membranes and quaternized polypropylene membranes in the hydroxide form at room temperature, 30 % RH

sample	Tensile strength (MPa)	Young's modulus (MPa)	Elongation at break (%)
PP	35±5	1285±125	458±82
PP-Br-20	21±4	785±65	346±55
PP-TMA-20	17±5	635±55	328±48
PP-DMHDA-20	16±4	588±45	312±45
nx-PP-Br-20	19±4	751±60	315±65
x-PP-TMA-20	62±5	1588±155	233±47
x-PP-DMHDA-20	64±5	1627±162	216±42

Water Uptake Behaviors and Dimensional Swelling

Water uptake (WU) of AEMs is an important parameter for IEC, ionic conductivity, dimensional stability, mechanical strength and membrane electrode compatibility. Table 3 compares the IEC, water uptake, swelling ratio in the in-plane direction of the PP-based membranes. Generally, the water uptake of membranes increased with IEC value, due to increased hydrophilicity. The highest water uptake was 36.5 wt % at 20 °C for the highest IEC membrane PP-DMHDA-20 (1.48 meq g^{-1}). The WU value was much lower than those of quaternized polyethylene (IEC=1.29 meq g^{-1}, WU = 97 wt %)[34] and aromatic copolymers.[35] The number of absorbed water molecules per quaternary ammonium (QA) group, the hydration number λ, was calculated to be lower than 14, which is also much lower than that of the quaternized polyethylene (λ=41.8).[36] The lower water uptakes are considered to be related to the hydrophobicity of the long alkyl chain and the 'side-chain-type' architecture, which could contribute to suppression of excessive water uptake and swelling. Lower water uptake of PP-based membranes leads to lower dimensional swelling in water, as shown in Table 3. The in-plane water swelling ratio at 20 °C was less than 10 %. Moreover, the thermal crosslinking drastically lowered the water uptake and thus the dimensional swelling ratio of the materials (Table 3). Specifically, the crosslinked x-PP-TMA-20 membrane had a water uptake of 20.2 wt % and swelling ratio of 3.5 % at room temperature, which is significantly improved compared to the uncrosslinked PP-TMA-20 that absorbed 34 wt % water and swelled 8.1 % in water. These values are also lower than that of QA-PAES membrane.[35] At higher temperature (80 °C), the crosslinked membranes retained excellent dimensional stability with equal to or less than 25 wt % water uptake and 6 % swelling ratio, as shown in Fig. 6. Considering the remarkable agreement between the high solvent resistance and low swelling ratio, a strong covalent crosslinking network was likely formed by thermal crosslinking, which was further confirmed by the high gel fraction as mentioned above. The low in-plane swelling is beneficial in reducing mechanical failures in the membrane electrode assembly (MEA), since high in-plane swelling deforms the membrane electrode interface. Unlike several other previously reported AEMs in which higher temperature induced excessive water uptake and dimensional swelling, the water uptake and swelling ration of PP AEMs shown very low dependence on temperature, as shown in Fig. 6. These results indicated that the 'side-chain-type' from hydrophobicity of spacer alkyl chain restricts water absorption of membranes more efficiently at higher temperatures.

Cite this: DOI: 10.1039/c0xx00000x

www.rsc.org/xxxxxx

ARTICLE TYPE

Table 3 Physico-chemical properties of PP based AEMs at room temperature (20 °C).

Samples	IEC[a]	IEC[b]	WU (wt %)	Swelling (%)	λ	MU[c] (wt %)	P_{MeOH} ($\times10^{-7}$ cm^2 s^{-1})	σ (mS cm^{-1})
PP-DMHDA-7	0.87	1.26	8.3	2.4	8.9	7.1	0.17	6.1
PP-TMA-20	1.56	2.57	34.0	8.1	12.1	31.2	2.19	17.4
PP-DMHDA-20	1.48	1.66	36.5	8.4	13.7	32.8	2.48	19.2
x-PP-TMA-20	1.34	2.33	20.2	3.5	8.4	16.2	0.39	14.6
x-PP-DMHDA-20	1.42	1.65	21.1	3.8	8.3	17.2	0.45	16.3
QA-PE[55]	1.2		97.0	--	41.8	--	--	40.0
QA-PAES[56]	1.82		20.0	11	5.7	--	--	22.0
QA-PPOs[28]	1.39		25.9	7	10.4	--	--	4.0

[a] measured by titration (meq. g^{-1}); [b] theoretical IEC values (meq. g^{-1}); [c] methanol uptake (MU) at 20 °C.

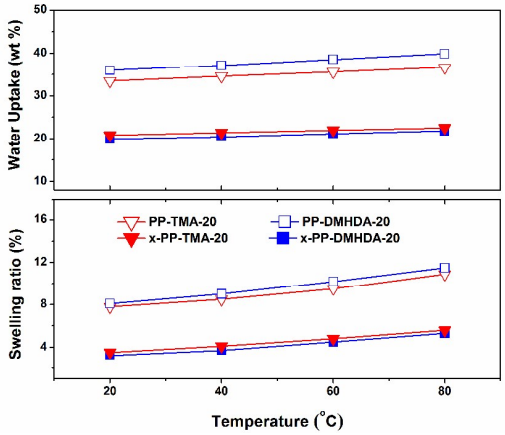

Fig. 6 The dependence of water uptake and swelling ration on temperature.

Hydroxide Conductivity

Hydroxide conductivity is a critical performance metric for AEMs. There is a requirement for the hydroxide conductivity to be above 10 mS·cm^{-1} and for water uptake to be less than 30 wt %. The hydroxide conductivity of the PP-based AEMs was measured in water and compared with that of QA-PPO and PE-based AEMs, and reported in Table 3 are expressed in Fig. 7a as a function of IEC. These values were above 10 mS cm^{-1} at 20 °C. The PP-DMHDA-20 membrane having a water uptake of 36.5 wt % achieved the highest hydroxide conductivity of 19.2 mS cm^{-1} at 20 °C. The important point to note is that the crosslinked membranes showed a much lower water uptake but a comparable conductivity value to the uncrosslinked PP-based AEMs (Table 3 and Fig. 7a). For example, the crosslinked x-PP-DMHDA-20 exhibits a hydroxide conductivity of 16.3 mS cm^{-1}, although its water uptake is only 21.1 wt %. While lower hydroxide conductivities was observed for PP-AEMs than that of QA-PE at a similar IEC value, the PP-AEMs displayed higher water uptake normalized-hydroxide conductivity than that of traditional QA-PPO and PE-based AEMs (Fig. 7b) if the water uptake of AEMs is taken into account. Particularly, the crosslinked x-PP-DMHDA-20 membranes exhibited extremely high normalized-hydroxide conductivity of 1.96 mS·cm^{-1}. This value is much higher than that of QA-PPO[8] and QA-PE[34] (0.38 and 0.96 mS cm^{-1}, respectively). Thus, it is believed that the side-chain-type architecture in PP-based AEMs contributes strongly to the high hydroxide conducting. The side-chain-type structure induces the PP-based AEMs to utilize water molecules more efficiently for hydroxide transport. As shown in Fig. S7, the polymers showed obvious characteristic ionomer peaks in the SAXS, indicating the formation of nanophase separation with ionic domains. These results suggest that our concept to apply the 'side-chain-type' structure is effective for the AEMs for mitigating water swelling and improving conductivity. However, both the hydroxide conductivities and water uptake normalized-hydroxide conductivities are much lower than those of QA-PAES AEM[35] with few exception[37] in spite of their similar IEC value. This is because the PP-based AEMs were fabricated by a hot-press process of non-ionic bromoalkylated PP membrane and subsequent amination reaction. Well-defined microphase separation is hard to form for hydroxide transport during the hot-press of non-ionic bromoalkylated PP membranes. The lack of a second order scattering peak for all membranes in SAXS results (Fig. S7) suggests that the arrangement of the phase separated domains is only locally correlated, and no long-range ordered structures formed in these materials. The correlation between hydroxide conductivity and temperature for PP-based AEMs is shown in Fig. 8. The conductivity steadily increased with temperature due to enhanced water mobility, which allows transport of hydroxide ions by the vehicle mechanism. The hydroxide conductivity values of 51.8–58.2 mS cm^{-1} for PP-AEMs are comparable to the reported values for polysulfone-based AEMs having high IEC values (IEC>2 meq g^{-1}).[35]

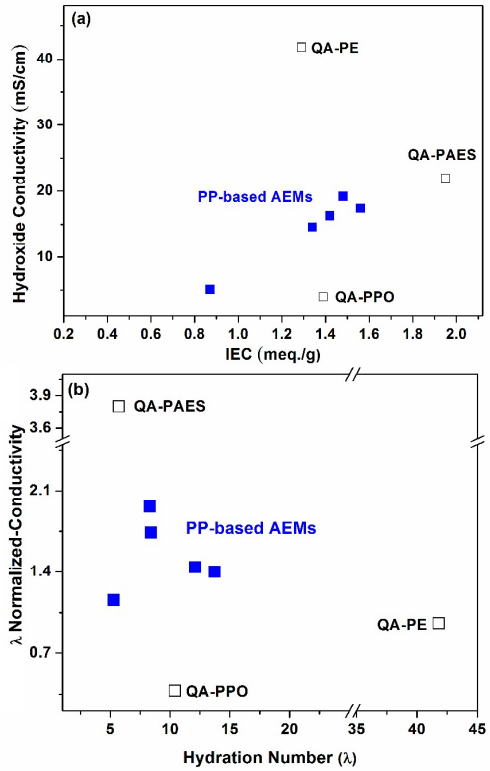

Fig. 7 (a) Conductivity of PP-based AEMs, QA-PE[55], QA-PAES[56] and QA-PPO[28] membranes at 20 °C as a function of IEC values; (b) the number of absorbed water molecules per quaternary ammonium (QA) group (λ) normalized hydroxide conductivity of AEMs as a function of the hydration number (λ).

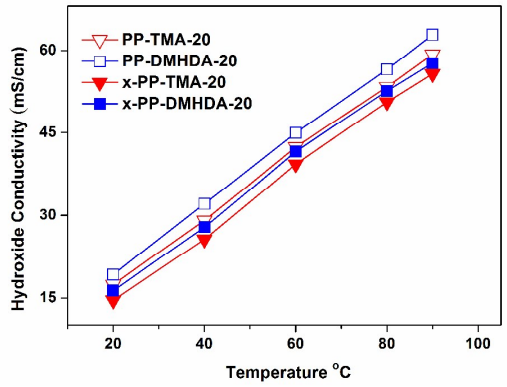

Fig. 8 Hydroxide conductivity of PP-based AEMs as a function of temperature.

Methanol Uptake and Permeability

Methanol can be used as fuel in solid alkaline fuel cells, thus methanol permeability is one of the key parameters to evaluate AEMs for alkaline fuel cells application. Methanol permeability is the product of the diffusion coefficient and the sorption coefficient and is used to describe the transport of methanol through membranes. Diffusion or leakage of the fuel across the membrane from anode to cathode leads not only to power loss from mixed potentials, but also other undesirable consequences, such as complicated water and thermal management. Thus, high methanol uptake or crossover is a serious obstacle for membranes in direct methanol fuel cell (DMFC) applications. Nafion has good conductivity due to strongly interconnected ionic domain morphology and high proton mobility, but its high methanol permeability is a shortcoming in its application in DMFC. Thus, many strategies have been developed to decrease methanol uptake and permeability in polymer electrolyte membranes, including using hydrocarbon polymer backbone, crosslinking etc.

As shown in Table 3, the highest methanol uptake of PP-based AEMs was ~32.8 %, which is much lower than that of Nafion 212 (103 %) at 20 °C. The methanol permeabilities of PP-based AEMs were also measured at 20 °C in 2 M aqueous methanol. The PP-based AEMs exhibited comparatively lower methanol permeability to Nafion, as shown in Fig. 9. The permeability values for 2 M methanol at room temperature were in the range of 0.17×10^{-7} to 2.48×10^{-7} cm^2 s^{-1}, which is almost one order of magnitude lower than that of Nafion (1.67×10^{-6} cm^2 s^{-1}). Although the PP-based AEMs have lower conductivities than Nafion, the hydroxide conductivities are sufficiently high to achieve much better selectivity, which is the ratio of ion conductivity to methanol permeability (Fig. 9). Moreover, the crosslinked PP-based AEMs x-PP-TMA and x-PP-DMHDA showed decreased methanol permeability and increased selectivity when compared with the uncrosslinked counterpart, as shown in Fig. 9. These results indicate that the crosslinked AEMs help reduce methanol permeability while retaining effective hydroxide transport.

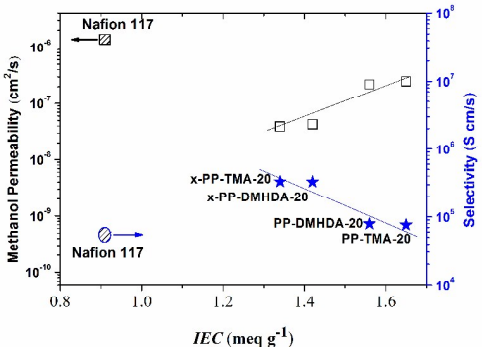

Fig. 9 Relationship of methanol permeability with hydration number (λ) and IEC values of membranes.

Alkaline stability

The long-term stability of AEMs is of concern due to well-known degradation pathways for tetraalkylammonium ions under alkaline conditions including beta-hydrogen Hofmann elimination, direct nucleophilic substitution at an alpha-carbon, or nitrogen ylide formation.[4, 38–40] The alkaline stability of the PP-based AEMs was determined by observing changes in conductivities and IEC values with time in 5 M and 10 M NaOH solution at 80 °C for 700 h. All of the membranes remained tough and flexible throughout the test due to the exceptional stability of the polyproplyene backbone. As shown in Fig. 10, the decreases in conductivity are all accompanied by similar decreases in IEC, confirming that the conductivity losses are due to cation degradation. After an initial period of rapid conductivity decline over the first 100 h, the IEC values and hydroxide conductivities of all membranes showed a slow, steady decline, as seen in Fig. 10. The enhanced stability behavior, which is similar with our previous AEMs based on PPO, might be due to steric shielding of cationic domains with alkyl chains. This finding is supported by the alkaline stability of PP-based AEMs containing an extended

alkyl chain (DMHDA). For example, the PP-DMHDA-20 membrane in 5 M aqueous NaOH showed a lower hydroxide conductivity drop of ~ 10 % in the initial 100 h testing period than that of PP-TMA-20 membrane (~18 %). Moreover, improved alkaline stability was observed for crosslinked x-PP-DMHDA-20 compared to non-crosslinked PP-DMHDA-20 (Fig. 10a). While the PP-DMHDA-20 showed a gradual decrease in hydroxide conductivity of about ~13 % over the 700 h test, crosslinked x-PP-DMHDA-20 showed only a ~ 5 % drop, as shown in Fig. 10a. The IEC values of the PP-based AEMs changed little during the stability testing period (Fig. 10b), which further confirms their improved alkaline stability. It is interesting to note that the PP-based AEMs retained more than 85 % of their initial hydroxide conductivity even under very severe conditions (80 ^{o}C, 10 M aqueous NaOH), as shown in Fig. 10c, despite the fact that the cations are susceptible to Hofmann elimination reactions. The comparison of FT-IR results for x-PP-DMHDA-20 membrane before and after alkaline stability testing in 10 M NaOH aqueous provides further evidence supporting its excellent alkaline stability. As shown in Fig. S3, no obviously variation in intensity of absorption bands of C–N and –OH etc was observed after 700 h testing. This finding is supported by a recent computational study using model compounds, which revealed that the attachment of quaternary ammonium groups to the polymer backbone having an alkyl spacer of > 3 carbon atoms can lead to improved alkaline stability of the cation.[36] This stability is the result of both steric shielding of the β-hydrogens when n > 3 and an increased susceptibility to *SN*^{2} attack at the non-methyl substituent on the nitrogen atom in BTMA. A similar stability result for a poly(phenylene) backbone with "side-chain-type" trimethylalkylammonium cations attached by a hexamethylene spacer was also reported by Hibbs.[13] In addition to the "side-chain-type" architecture, the highly base-stable PP backbone likely also contributes to the excellent alkaline stability of PP-based AEMs; previous reports by Hickner and coworkers[15] shown that base stable polymer backbone would induce a better alkaline stability of AEMs. Thus, the PP-based AEMs with "side-chain-type" cations appear to be very promising candidate for use in AEMFCs.

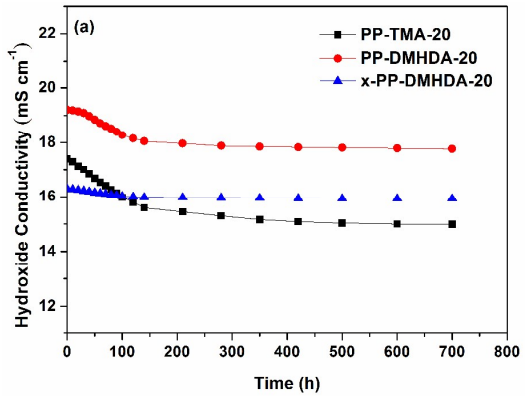

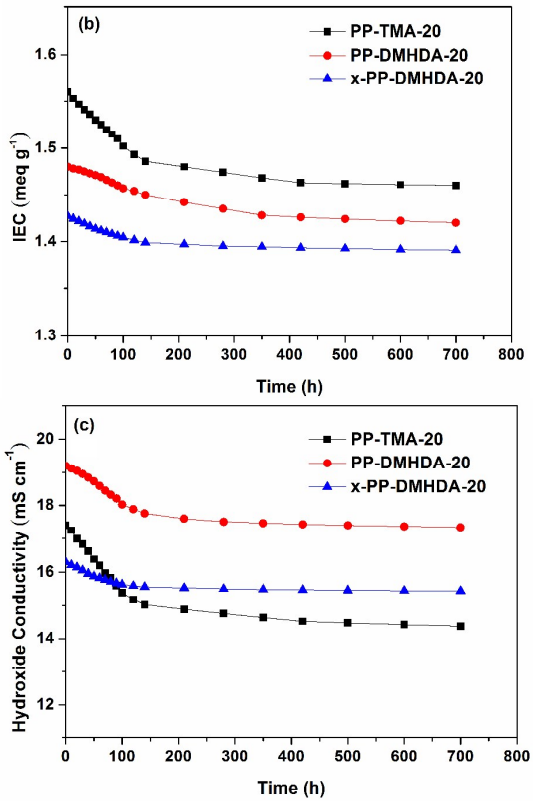

Fig. 10 The changing trend for PP-based AEM membranes after immersion at 80 °C in (a) hydroxide conductivity and (b) IEC in 5 M NaOH, and (c) hydroxide conductivity in 10 M NaOH.

Fuel Cell Performance

Figure 11 shows the initial polarization curves of an H_2/O_2 AEMFC with PP-TMA-20 as electrolyte membrane. The open circuit voltages (OCVs) are close to the theoretical value of about 1.1 V, indicating that the PP-TMA-20 membrane do not affect the catalyst function of Pt significantly. The peak power density for the AEMFC with the PP-TMA-20 membrane was 122 mW cm^{-2}. The higher power density and smaller internal resistance indicate that the side-chain type PP AEM is a promising electrolyte membrane that shows solubility in low-boiling-point solvents for membrane processing, but is insoluble during alkaline fuel cell operation.

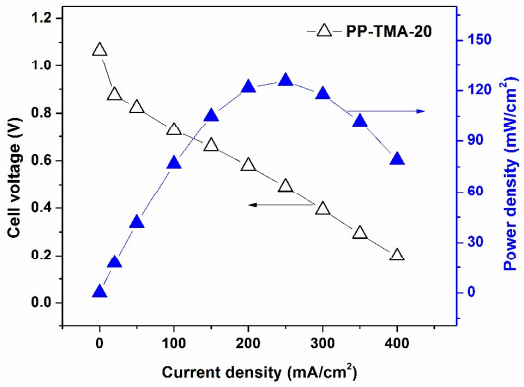

Fig. 11 Polarization curves (open symbols) and power density curves (filled symbols) of PP-TMA-20 membrane incorporated

AEMFC. Test conditions: membrane-thickness of 45 μm, cell temperature of 50 °C, catalyst loadings of 0.5 mg Pt cm^{-2} (Pt/C) for both anode and cathode, gas flow rate of 0.5 L min^{-1} for both H_2 and O_2.

Conclusions

We have designed and synthesized "side-chain-type" polypropylene-based anion exchange membrane with high base stability using heterogeneous Ziegler-Natta catalyst mediated polymerization that provide multiple structural variations to allow tuning of the membrane properties. The side chain type PP-based AEMs exhibited comparable hydroxide conductivity to typical AEMs based on benzyltrimethyl ammonium motif in spite of their low water uptake. The PP-based AEMs had unusually high alkaline stability for up to 700 h in 5 M and 10 M NaOH at 80 °C. The steric effects of the long alkyl chains in 'side-chain-type' architecture surrounding the quaternary ammonium center are likely the cause of the observed good alkaline stability. Crosslinkable PP-based AEMs were also obtained simply by copolymerization of a thermally crosslinkable monomer. All of the crosslinked membranes had better overall properties including lower water uptake, lower water swelling ratio, better mechanical properties, and lower methanol permeability, compared to those of the uncrosslinked counterparts, while having comparable hydroxide conductivities. A combination of good thermal and chemical stability, excellent mechanical properties and excellent balance between hydroxide conductivity and swelling or methanol transport makes PP-based membrane attractive as AEM materials for alkaline fuel cells applications. We consider that these 'side-chain-type' polypropylene synthesized by commercial heterogeneous Ziegler-Natta catalyst mediated polymerization could lead to new materials for the production of AEMs that meet the demanding challenges of alkaline fuel cells and other electrochemical processes. The general approach is versatile for varying the length of the side-chain and the cations, which may be lead to further tuning and refinement of AEMs to address the various separations and energy-focused applications.

Acknowledgement

This work was supported by the National Natural Science Foundation of China under Grant 21404084 and 21474126, and by the State Key Laboratory of Solidification Processing in NWPU (Grand No. G8QT0298) and the 111 Project (B08040).

Notes and references

[a] *State Key Laboratory of Solidification Processing, Northwestern Polytechnical University, Xi'an, 710072, China. E-mail: wangyiguang@nwpu.edu.cn*

[b] *State Key Laboratory of Coal Conversion, Institute of Coal Chemistry, Chinese Academy of Sciences, Taiyuan, 030001, China. E-mail: linanwen@sxicc.ac.cn*

[c] *Department of Materials Science and Engineering, Advanced Materials Processing and Analysis Center, University of Central Florida, Orlando, FL 32816, USA*

[d] *State Key Laboratory of Engines, School of Mechanical Engineering, Tianjin University, Tianjin 300072, China*

[e] *Collaborative Innovation Center of Chemical Science and Engineering (Tianjin), Tianjin 300072, China*

† Electronic Supplementary Information (ESI) available: See DOI: 10.1039/b000000x/

1 F. Zhang, H. Zhang and C. Qu, *J. Mater. Chem.,* 2011, **21**, 12744–12752.
2 K. D. Kreuer, *Chem. Mater.,* 1996, **8**, 610–641.
3 W. Li, J. Fang, M. Lv, C. Chen, X. Chi, Y. Yang and Y. Zhang, *J. Mater. Chem.,* 2011, **21**, 11340–11346.
4 G. Merle, M. Wessling and K. Nijmeijer, *J. Membr. Sci.,* 2011, **377**, 1–35.
5 J. S. Spendelow and A. Wieckowski, *Phys. Chem. Chem. Phys.,* 2007, **9**, 2654–2675.
6 J. Pan, S. Lu, Y. Li, A. Huang, L. Zhuang and J. Lu, *Adv. Funct. Mater.,* 2009, **19**, 1–8.
7 N. Li, L. Wang and M. A. Hickner, *Chem. Comm.,* 2014, **50**, 4092–4095.
8 N. Li, T. Yan, T. Thurn-Albrecht and W. H. Binder, *Energy. Environ. Sci.,* 2012, **5**, 7888–7892.
9 N. Li, Y. Leng, M. A. Hickner and C.-Y. Wang, *J. Am. Chem. Soc.* 2013, **135**, 10124–10133.
10 T. Xu, D. Wu and L. Wu, *Prog. Polym. Sci.,* 2008, **33**, 894–915.
11 J. Miyake, K. Fukasawa, M. Watanabe, K. Miyatake, *J. Polym. Sci., Polym. Chem.,* 2014, **52**, 383–389.
12 L. Wang and M. A. Hickner, *Polym. Chem.*, 2014, **5**, 2928–2935.
13 M. R. Hibbs, *J. Polym. Sci., Polym. Phys.,* 2013, **51**, 1736–1742.
14 C. G. Arges and V. Ramani, *Proc. Natl. Acad. Sci. U.S.A.* 2013, **110**, 2490−2495.
15 S. A. Nuñez and M. A. Hickner, *ACS Macro Lett.*, 2013, **2**, 49–52.
16 B. Bae, B. H. Chun and D. Kim, *Polymer,* 2001, **42**, 7879–7885.
17 G. Venugopal, J. Moore, J. Howard and S. Pendawar, *J. Power Sources.,* 1999, **77**, 34–41.
18 H. Matsuyama, M. Yuasa, Y. Kitamura, M. Teramoto and D. R. Lloyd, *J. Membr. Sci.,* 2000, **179**, 91–100.
19 G. K. Kostov and S. C. Turmanova, *J. Appl. Polym. Sci.,* 1997, **64**, 1469–1475.
20 W. M. Trochimczuk, *J. Polym. Sci.: Polym. Chem. Ed.,* 1975, **13**, 357–363.
21 S. M. Kolhe and A. Kumar, *Radiat. Phys. Chem.,* 2005, **74**, 384–390.
22 T. C. Chung, *Functionalization of Polyolefins*; Academic Press: London, 2002.
23 T. C. Chung, *Prog. Polym. Sci.,* 2002, **27**, 39–85.
24 G. Ruggeri, M. Aglietto, A. Petragnani and F. Ciardelli, *Euro. Polym. J.,* 1983, **19**, 863–866.
25 M. Zhang, H. K. Kim, E. Chalkova, F. Mark, S. N. Lvov and T. C. Chung, *Macromolecules,* 2011, **44**, 5937–5946.
26 M. Zhang, X. Yuan, L. Wang, T. C. Chung, T. Huang and W. deGroot, *Macromolecules,* 2014, **42**, 571–581.
27 T. J. Clark, N. J. Robertson, H. A. Kostalik, E. B. Lobkovsky, P. F. Mutolo, H. D. Abruña and G. W. Coats, *J. Am. Chem. Soc.,* 2009, **131**, 12888–12889.
28 N. J. Robertson, H. A. Kostalik, T. J. Clark, P. F. Mutolo, H. D. Abruña and G. W. Coats, *J. Am. Chem. Soc.,* 2010, **132**, 3400–3404.
29 C. Natta, *J. Polym. Sci.,* 1960, **48**, 219–239.
30 R. Bacskai, *J. Polym. Sci: Part A.,* 1965, **3**, 2491–2510.
31 W. Lin, Z. Shao, J. Dong and T. C. Chung, *Macromolecules,* 2009, **42**, 3750–3754.
32 M. R. Hibbs, M. A. Hickner, T. M. Alam, S. K. Mcintyre, C. Fujimoto, J. Cornelius, *Chem. Mater.,* 2008, **20**, 2566–2573.
33 M. Tanaka, M. Koike, K. Miyatake and M. Watanabe, *Polym. Chem.* 2011, **2**, 99−106.
34 H. A. Kostalik, T. J. Clark, N. J. Robertson, P. F. Mutolo, J. M. Longo, H. D. Abruña and G. W. Coates, *Macromolecules,* 2010, **43**, 7147–7150.
35 J. Wang, J. Wang, S. Li and S. Zhang, *J. Membr. Sci.,* 2011, **368**, 246–253.
36 S. Chempath, J. M. Boncella, L. R. Pratt, N. Henson and B. S. Pivovar, *J. Phys. Chem. C*., 2010, **114**, 11977−11983.
37 N. Li, Q. Zhang, C. Wang, Y. M. Lee, M. D. Guiver, *Macromolecules*, 2012, **45**, 2411–2419.
38 J. R. Varcoe, P. Atanassov, D. R. Dekel, A. M. Herring, M. A. Hickner, P. A. Kohl, A. R. Kucernak, W. E. Mustain, K. Nijmeijer, K. Scott, T. W. Xu and L. Zhuang, *Energy. Environ. Sci.,* 2014, **7**, 3135–3191.

39 N. Li and M. D. Guiver, *Macromolecules* 2014, **47**, 2175–2198.
40 A. D. Mohanty and C. Bae, *J. Mater. Chem. A*., 2014, **2**, 17314–17320.
41 W. Chiu and S. Fang, *J. App. Polym. Sci.,* **1985,** *30,* 1473-1489.
42 T. Xu, F. Zhang, *J. Membr. Sci.* **2002**, *199*, 203-210.
43 J. Qiao, J. Fu, L. Liu, Y. Liu, J. Sheng, *Int. J. Hydrogen Energy,* **2012**, *37*, 4580-4589.

"Side-chain-type" and crosslinkable quaternized polypropylene was prepared by heterogeneous Ziegler-Natta catalyst mediated polymerization for highly stable anion exchange membranes